JGR Atmospheres

RESEARCH ARTICLE
10.1029/2025JD044260

Special Collection:
Land-atmosphere coupling: measurement, modelling and analysis

Dynamic Modeling of Ammonia Emissions and Nitrogen Deposition via Online Coupling of WRF-Chem and Noah-MP-CN

Yeer Cao[1,2], Chuanhua Ren[3], Han Zhang[1], Zhongwang Wei[1], Yixin Guo[4], and Xitian Cai[2]

[1]School of Atmospheric Sciences, Sun Yat-Sen University, Guangzhou, China, [2]School of Civil Engineering, Sun Yat-Sen University, Guangzhou, China, [3]Joint International Research Laboratory of Atmospheric and Earth System Sciences, School of Atmospheric Sciences, Nanjing University, Nanjing, China, [4]Earth, Ocean and Atmospheric Sciences Thrust, Function Hub, Hong Kong University of Science & Technology (Guangzhou), Guangzhou, China

Abstract Ammonia (NH_3) is an important alkaline gas, mainly emitted from agricultural activities, playing an important role in global nitrogen cycle and surface ecosystems. Chemical transport models and emission inventories are widely used to study the emission, transport, and chemical transformation of NH_3. However, traditional static inventories consider emissions as unidirectional, overlooking interactions between NH_3 emissions and other ecosystems, especially land surface processes linked to emissions. In this study, we achieved bidirectional NH_3 exchange between land surface and atmospheric chemistry models by developing WRF-CN-Chem, a model integrating the Noah-MP land surface model with carbon-nitrogen dynamics (Noah-MP-CN) and the Weather Research and Forecasting model with atmospheric chemistry (WRF-Chem). Compared with the static Multi-resolution Emission Inventory for China, the dynamic bidirectional model exhibits higher spatiotemporal resolution and demonstrated a stronger temporal correlation with satellite observations. WRF-CN-Chem model estimated 7.88 TgN NH_3 emission in year 2020 in eastern China. Additionally, we incorporated the atmospheric nitrogen deposition, simulated by the "Online" experiment, into the soil ammonium pool. Our findings revealed an increase of 2.25 TgC yr^{-1} in land net primary productivity (NPP) in eastern China attributable to the increased nitrogen deposition. By incorporating bidirectional NH_3 exchange between land surface and atmosphere chemistry models, this study enhances the simulation of dynamic ammonia emissions and improves understanding of atmospheric nitrogen deposition processes. Furthermore, linking these processes to land NPP provides valuable insights for sustainable land management and pollution mitigation strategies, helping address the environmental impacts of excessive fertilization.

Plain Language Summary Ammonia, a common harmful gas emitted from agricultural croplands, plays a crucial role in global nitrogen cycles through NH_3 volatilization. Previous studies have often regarded NH_3 emission as a static process in air quality modeling, relying on emission inventories with limited spatial and temporal resolutions, thus failing to investigate the complete terrestrial and atmospheric nitrogen cycle. We integrated the land surface and chemistry modules into the regional climate model WRF. Leveraging the nitrogen dynamics module (Noah-MP-CN), our novel emission strategy enables a more accurate representation of annual variations in NH_3 emission fluxes, including the dynamic deposition of reduced nitrogen (NH_3 and NH_4^+) onto the land surface. Additionally, we assessed the effects of nitrogen deposition on vegetation growth, revealing a 2.25 TgC yr^{-1} reduction in NPP in the absence of nitrogen deposition.

Key Points:

- We achieved dynamic modeling of NH_3 emission and atmospheric N deposition via bidirectional coupling between Noah-MP-CN and WRF-Chem
- Dynamic ammonia emissions show a stronger temporal correlation with satellite observations than static inventories
- The model quantifies a significant increase in land net primary productivity driven by nitrogen deposition feedback

Supporting Information:

Supporting Information may be found in the online version of this article.

Correspondence to:

X. Cai,
caixitian@mail.sysu.edu.cn

Citation:

Cao, Y., Ren, C., Zhang, H., Wei, Z., Guo, Y., & Cai, X. (2026). Dynamic modeling of ammonia emissions and nitrogen deposition via online coupling of WRF-Chem and Noah-MP-CN. *Journal of Geophysical Research: Atmospheres*, *131*, e2025JD044260. https://doi.org/10.1029/2025JD044260

Received 2 MAY 2025
Accepted 12 JAN 2026
Corrected 11 FEB 2026

This article was corrected on 11 FEB 2026. See the end of the full text for details.

Author Contributions:

Conceptualization: Yeer Cao, Chuanhua Ren, Xitian Cai
Data curation: Yeer Cao
Formal analysis: Yeer Cao, Xitian Cai
Investigation: Yeer Cao, Xitian Cai
Methodology: Yeer Cao, Chuanhua Ren

1. Introduction

Ammonia (NH_3), a key alkaline pollutant, directly influences atmospheric chemistry and participates in the global nitrogen cycle. Excessive NH_3 emissions contribute to severe environmental challenges, including reactions with acidic gases such as H_2SO_4 and HNO_3 to form ammonium aerosols (Xiao Fu et al., 2017) and elevate global $PM_{2.5}$ concentration (Gu et al., 2021). Human activities, particularly the widespread use of synthetic nitrogen fertilizers to enhance crop yields and sustain nearly half the global population (Erisman et al., 2008), have made agricultural lands the largest anthropogenic source of NH_3 emissions (Ma et al., 2021). Global nitrogen fertilizer application rates surged from 10 Tg N yr^{-1} in 1961 to 77 Tg N yr^{-1} in 2016 (Martínez-Dalmau et al., 2021), intensifying risks of soil acidification, water eutrophication, biodiversity loss (Han et al., 2019), and elevated atmospheric nitrous oxide levels. Reactive nitrogen (Nr) emissions, including NH_3, directly and indirectly impact climate change (Bhautmage et al., 2022) through altering regional and global radiative forcing, terrestrial and marine primary

Resources: Yeer Cao, Xitian Cai
Software: Yeer Cao, Chuanhua Ren
Supervision: Zhongwang Wei, Xitian Cai
Validation: Yeer Cao, Xitian Cai
Visualization: Yeer Cao
Writing – original draft: Yeer Cao
Writing – review & editing: Chuanhua Ren, Han Zhang, Zhongwang Wei, Yixin Guo, Xitian Cai

production, and terrestrial feedback mechanisms. Under high-warming climate scenarios, NH_3 emissions are projected to increase by 84% by 2,100 and reduce crop production by 540 Gg N yr^{-1} in the U.S (Shen et al., 2020).

Importantly, the chemical balance governing atmospheric NH_3 is shifting. As successful air quality policies in China have reduced SO_2 and NOx emissions, the atmospheric capacity to neutralize ammonia has decreased, which can lead to an increase in ambient gaseous NH_3 concentrations (Lachatre et al., 2019). This feedback makes accurate, dynamic modeling of NH_3 emissions more critical than ever. Consequently, such simulations are crucial for advancing our understanding of the nitrogen cycle, aerosol–radiation feedback, and air quality forecasting.

Emission inventories, employed as a "bottom-up" approach in chemical transport models, have been widely used to study ammonia emissions globally, for example, the MASAGE_NH_3 inventory of Paulot et al. (2014), regionally in China (Kang et al., 2016; L. Zhang et al., 2018), and locally in the Pearl River Delta (J. Y. Zheng et al., 2012). These inventories link emissions to elevated $PM_{2.5}$ (W. Xu et al., 2022) and increased nitrogen deposition (Y. Chen et al., 2021). However, their accuracy depends heavily on input data quality, including agricultural activity levels, emission factor parameterization, meteorological conditions, and agricultural management. However, the rather limited spatiotemporal resolution of input data for inventory development and relatively simplified parameterization of emission factors hinder the characterization of fine-scale emission details and land-atmosphere feedbacks.

Recent advances focus on dynamic emission modeling. Werner et al. (2017) demonstrated that incorporating dynamic NH_3 emissions in the WRF-Chem model reduced seasonal mean gross errors in Europe compared to static inventories. Similarly, Chuanhua Ren et al. (2023) developed a dynamic ammonia emission model named WRF-SoilN-Chem v1.0, which combines meteorological variables and static emission data to estimate real-time NH_3 emission fluxes. The evaluation demonstrates a significant enhancement in the model's performance for capturing measured NH_3 flux and ambient concentrations in China. Machine learning approaches, such as the random forest algorithm by P. Xu et al. (2024), have further refined global NH_3 emission factors, revealing rice, wheat, and maize contributions of 41.1%, 30.2%, and 28.7%, respectively, to total agricultural emissions (4.3 Tg N).

Ammonia volatilization is a crucial process in the nitrogen cycle, serving as a key factor in the exchange of substances between the land surface and the atmosphere. Terrestrial nitrogen dynamics-related processes are increasingly being incorporated into climate and Earth system models (Asaadi & Arora, 2021; Davies-Barnard et al., 2020; Gerber et al., 2010; Shi et al., 2016; Zaehle & Friend, 2010). However, few land surface models explicitly link nitrogen cycling to atmospheric interactions, particularly bidirectional emission-deposition feedback. For instance, Bash et al. (2013) integrated the CMAQ v5.0 model with the Environmental Policy Integrated Climate (EPIC) agroecosystem model and performed a sensitivity experiment in the Continental US (CONUS). This study applied a aerodynamic resistance based NH3 flux calculation method and successfully captured the bidirectional exchange and improved simulations of the reduced nitrogen (NH_3 + NH_4^+) wet deposition and ambient aerosol concentrations. Similarly, X Fu et al. (2015) employed the CMAQ-EPIC model along with fertilization data to estimate NH_3 emissions in China with enhanced spatial and temporal resolutions. While pioneering, the CMAQ-EPIC framework represents a "loosely coupled" system, requiring separate runs and offline data processing to link the Weather Research and Forecasting (WRF) meteorological model, the EPIC agroecosystem model, and the CMAQ chemistry transport model. The bidirectional flux is calculated within CMAQ using a resistance-based scheme dependent on a canopy compensation point. In contrast, our WRF-CN-Chem approach offers a fully online, two-way coupled integration entirely within the WRF framework. Here, the NH_3 flux is calculated directly within the process-based Noah-MP-CN land surface model and is exchanged with the WRF-Chem atmospheric model at each timestep. This unified architecture provides a more seamless and computationally efficient method for simulating the dynamic feedbacks between the land surface nitrogen cycle and atmospheric chemistry.

Nitrogen deposition plays a critical role in shaping terrestrial/aquatic ecosystems, driving aquatic eutrophication (Cornell et al., 2003) and modulating carbon sequestration (Reay et al., 2008). Additionally, feedback mechanisms between nitrogen deposition and ammonia emissions influence total ammonia emissions (Zhu et al., 2015), underscoring the need to incorporate dynamic deposition processes into climate models. For instance, Zhu et al. (2015) utilized the GEOS-Chem model to simulate global-scale bidirectional exchange of ammonia and diurnal variation in livestock emissions. They improved the static emission inventory by implementing a redesigned diurnal variation scheme and incorporating a soil ammonia pool for bidirectional nitrogen exchange.

Similarly, Vira et al. (2022) developed the Flow of Agricultural Nitrogen model within the Community Land Model and combined it with the CAM-chem model, which represents the land surface and chemistry components of the Community Earth System Model. They compared their NH_3 emission estimates against three global NH_3 emission inventories (EDGAR, CEDS, and HTAP), and evaluated performances for capturing observed atmospheric nitrogen deposition. However, CLM's nitrogen dynamics did not account for land surface nitrogen losses caused by ammonia emissions. Fung et al. (2022) advanced this field by integrating ammonia emissions and deposition into CESM2, combining nitrogen dynamics from CLM5 and CAM-Chem4 models. They quantified the impacts of NH_3 on atmospheric composition, its influence on Earth's radiation budget and biosphere, and the consequences of deposition on land surface NH_3 emissions. However, the analysis neglected the effects of nitrogen deposition on vegetation productivity.

Recent studies have increasingly focused on understanding bidirectional exchange between the soil and the atmosphere, particularly for nitrogen, a cross-media pollutant requiring integrated management. Nevertheless, current modeling frameworks face significant limitations. A primary issue lies in the reliance on global-scale models (e.g., GEOS-Chem, CAM-Chem), whose coarse spatial resolution hampers their capacity to depict the nuanced regional emission patterns accurately. Consequently, this limitation results in an inability to provide precise representations of localized variations in ammonia emissions, essential for addressing region-specific environmental challenges. Moreover, on a regional scale, the neglect of deposition feedback from the atmosphere at the lower boundary (land surface) represents a significant gap in current research. This oversight limits our understanding of the interconnected processes in the nitrogen cycle, ultimately neglecting the broader ecological implications. Specifically, the omission of deposition feedback leads to the exclusion of nitrogen loss and gain at the land surface, which may result in an inaccurate assessment of its impact on plant growth—a crucial factor in ecological systems.

To address these limitations, we propose the development of a novel regional-scale emissions and deposition model designed to overcome the constraints of existing global-scale models. By prioritizing high spatiotemporal resolution, our approach enables a more accurate representation of regional emission patterns and deposition processes, which are often obscured in coarse-resolution global models. By including deposition feedback at the regional level, our research endeavors to bridge significant knowledge gaps regarding nitrogen dynamics, thus promoting the development of more efficient environmental management strategies and offering valuable insights into the complex interplay between atmospheric processes and terrestrial ecosystems. Specifically, we coupled the Noah-MP-CN land surface model—an extension of Noah-MP that incorporates a coupled terrestrial carbon and nitrogen cycle module—with the WRF-Chem atmospheric chemistry model. Additionally, we made necessary adjustments to the terrestrial nitrogen cycle processes. To evaluate the model's performance, we conducted two experiments: one simulating dynamic emissions and deposition feedback, and another using static emissions for comparative analysis.

2. Methodology and Materials

2.1. WRF-Chem Framework for Dynamic Emission and Deposition

The WRF model is a non-hydrostatic compressible mesoscale atmospheric model that offers researchers a straightforward method for simulating weather and climate processes. WRF-Chem (Skamarock et al., 2019) is an extension of the WRF model that integrates atmospheric chemistry modules to enable simultaneous simulation of the emission, transport, deposition, and chemical transformation of trace gases and aerosols alongside meteorology. This framework is particularly valuable for studying regional-scale air quality, analyzing field programs, and examining the intricate interactions between clouds and chemistry at the cloud scale. For this study, we utilized WRF-Chem version 4.1.2.

2.2. Noah-MP-CN Land Surface Model With Nitrogen Dynamics

Noah-MP is a land surface model (LSM) based on Noah LSM, using multiple options for critical land-atmosphere interaction processes (Niu et al., 2011). As the default land surface scheme within the WRF framework, Noah-MP provides foundational simulations of surface energy, water, and carbon fluxes. To address nitrogen cycle dynamics, Noah-MP-CN was developed by X. Cai et al. (2016), integrating a terrestrial nitrogen (N) cycling module that simulates biological nitrogen fixation, plant nitrogen uptake, and soil nitrogen transformations. Noah-MP-CN partitions nitrogen into six distinct pools: soil active organic pool, fresh organic pool, stable organic pool,

residue organic pool, soil ammonium pool, and soil nitrate pool. The model resolves four vegetation-related nitrogen processes (i.e., active soil N uptake, passive soil N uptake, leaf N re-translocation, and symbiotic biological N fixation) and seven critical soil nitrogen cycle processes (i.e., mineralization, immobilization, decomposition, denitrification/nitrification, volatilization, nitrogen deposition, and nitrogen leaching). Noah-MP-CN has been successfully implemented in WRF version 4.1.2, demonstrating robust simulations of nitrogen cycle-atmosphere interactions (Xitian Cai et al., 2024).

Nitrogen mineralization is a key microbial process in the global N cycle, since it measures the absolute amount of ammonium (NH_4^+) produced from soil organic N due to microbial activity (Elrys et al., 2021) and increases NH_3 volatilization potential (H. Li et al., 2021). However, the original Noah-MP-CN model structure lacked explicit NH_4^+ sources from mineralization, relying instead on static nitrogen deposition and fertilization inputs. To address this, we modified the mineralization process by allocating 20% of nitrogen destined for the NO_3^- pool to the NH_4^+ pool in croplands (Plant Functional Types 12 and 14 under the Noah-IGBP land use classification). This adjustment improves NH_3 volatilization estimates by explicitly linking mineralization to NH_4^+ dynamics.

2.2.1. The Estimation of Ammonia Volatilization in Noah-MP-CN

Ammonia volatilization refers to the process of gaseous NH_3 loss from soils or surfaces. NH_3 emissions are strongly associated with soil temperature, soil moisture (Siman et al., 2020), wind speed (Zhan et al., 2020), precipitation events, and pH values (Huang et al., 2012). Three coefficients are used in the volatilization algorithms to account for the impact of these parameters. The volatilization regulator is calculated as:

$$\eta_{\mathrm{vol},ly} = \eta_{\mathrm{tmp},ly} \cdot \eta_{\mathrm{midz},ly} \cdot \eta_{\mathrm{cec},ly} \tag{1}$$

Where $\eta_{\mathrm{tmp},ly}$, $\eta_{\mathrm{midz},ly}$, $\eta_{\mathrm{cec},ly}$ are nitrification/volatilization temperature factor, volatilization depth factor, and volatilization cation exchange factor respectively. The total amount of nitrification and ammonia volatilization is calculated and then divided between the two processes. Nitrification is a function of soil temperature and soil water content, while ammonia volatilization is a function of soil temperature, depth, and cation exchange capacity. Nitrification/volatilization occurs only when the temperature of the soil layer exceeds 5°C.

The nitrification/volatilization temperature factor is calculated as:

$$\eta_{\mathrm{tmp},ly} = 0.41 \cdot \frac{(T_{\mathrm{soilly}} - 5)}{10} \text{ if } T_{\mathrm{soill},ly} > 5 \tag{2}$$

where $\eta_{\mathrm{tmp},ly}$ is the nitrification/volatilization temperature factor, and $T_{\mathrm{soil},ly}$ is the temperature of layer ly (°C).

The volatilization depth factor is given by:

$$\eta_{\mathrm{midz},ly} = 1 - \frac{z_{\mathrm{mid},ly}}{z_{\mathrm{mid},ly} + \exp[4.706 - 0.0305 \cdot z_{\mathrm{mid},ly}]} \tag{3}$$

where $\eta_{\mathrm{midz},ly}$ is the volatilization depth factor and $z_{\mathrm{mid},ly}$ is the depth from the soil surface to the middle of the layer (mm).

The volatilization cation exchange factor is set to a constant value:

$$\eta_{\mathrm{cec},ly} = 0.15 \tag{4}$$

The first-order kinetic rate equation determined the total amount of ammonium lost to nitrification and volatilization in layer ly, $N_{\mathrm{nit|vol},ly}$ (kg N m^{-2}), is calculated as follows:

$$N_{\mathrm{nit|vol},ly} = NH_{4,ly} \cdot \left[1 - \exp\left(-\eta_{\mathrm{nit},ly} - \eta_{\mathrm{vol},ly}\right)\right] \tag{5}$$

where $NH_{4,ly}$ is the amount of ammonium in layer ly (kg N m^{-2}), $\eta_{\mathrm{nit},ly}$ is the nitrification regulator, and $\eta_{\mathrm{vol},ly}$ is the volatilization regulator.

$N_{\mathrm{nit|vol},ly}$ is then divided into nitrification and volatilization. The amounts of N converted from NH_4^+ and NO_3^- of the ammonium pool via nitrification and volatilization are then calculated:

$$\begin{aligned} N_{\mathrm{nit},ly} &= \frac{fr_{\mathrm{nit},ly}}{\left(fr_{\mathrm{nit},ly} + fr_{\mathrm{vol},ll}\right)} \cdot N_{\mathrm{nit|vol},ly} \\ N_{\mathrm{vol},ly} &= \frac{fr_{\mathrm{vol},ly}}{\left(fr_{\mathrm{nit},ly} + fr_{\mathrm{vol},ly}\right)} \cdot N_{\mathrm{nit|vol},ly} \end{aligned} \tag{6}$$

where $fr_{\mathrm{nit},ly}$ and $fr_{\mathrm{nit},ly}$ are the estimated fractions of N lost through nitrification and volatilization, respectively. They are calculated as follows:

$$\begin{aligned} fr_{\mathrm{nit},ly} &= 1 - \exp\left[-\eta_{\mathrm{nit},ly}\right] \\ fr_{\mathrm{vol},ly} &= 1 - \exp\left[-\eta_{\mathrm{vol},ly}\right] \end{aligned} \tag{7}$$

The emission model calculates the NH_3 volatilization of all soil layers in Noah-MP-CN, total ammonia emission is the sum of all soil layers.

2.2.2. Feeding WRF-Chem Nitrogen Deposition to Noah-MP-CN

The nitrogen deposition process in Noah-MP-CN is empirical, it represents atmospheric wet deposition by combining timestep precipitation and yearly static historical data. For dry deposition, it only relies on static data input. WRF-Chem provides real-time atmosphere deposition data of all pollution gases, we take the NH_3 and NH_4^+ deposition generated by the WRF-Chem model and add the deposition to soil nitrogen pools in the LSM. WRF-Chem calculates dry deposition as follows:

$$\mathrm{DDFlux} = \frac{\mathrm{chem} * p}{R * T} * \mathrm{ddvel} * \Delta t * 10^{-6} \tag{8}$$

where DDflux is dry deposition flux, chem is the concentration of chemistry species, p is air pressure, R is the ideal gas constant, T is air temperature, ddvel is the dry deposition velocity, Δt is model time step, and 10^{-6} is a unit converting factor.

The dry deposition velocity (ddvel) is calculated using the resistance-based scheme of Wesely (2007). For aerosol dry deposition, we use the scheme by Binkowski and Shankar (1995). Wet scavenging, the process by which aerosols and gases are removed from the atmosphere by precipitation, plays a critical role in determining the lifecycle of atmospheric pollutants and their impacts on air quality and climate. To represent this process, we employ a multi-mechanism framework: In-cloud scavenging is simulated using the MOSAIC aerosol module (Easter et al., 2004), which resolves aerosol activation and removal within cloud droplets. Below-cloud scavenging follows the scheme of Slinn (1984), quantifying the collision and capture of aerosols by falling hydrometeors. Subgrid-scale convective scavenging is parameterized using the approach of Grell and Dévényi (2002), addressing removal processes in convective updrafts. These schemes collectively account for key scavenging mechanisms—including gas-phase reactions, aerosol-cloud interactions, and precipitation efficiency—to accurately model atmospheric pollutant concentrations and their spatiotemporal distributions. Text S1 in Supporting Information S1 describes the coupling of WRF-CHEM with Noah-MP-CN (Figure S1 in Supporting Information S1).

2.2.3. Experiment Design and Model Configuration

We coupled the chemistry and land surface models within WRF-Chem (detailed coupling processes are provided in Supporting Information S1) to better represent the bidirectional exchange of NH_x. Then we designed two experiments using the WRF-Chem model with and without dynamic emission module (hereafter referred to as WRF-CN-Chem).

The simulation domain (Figure 1) covers East Asia, including eastern China, with a 30-km spatial resolution, a 180-s model timestep, and 33 vertical layers extending to 50 hPa. A sub-region encompassing the North China

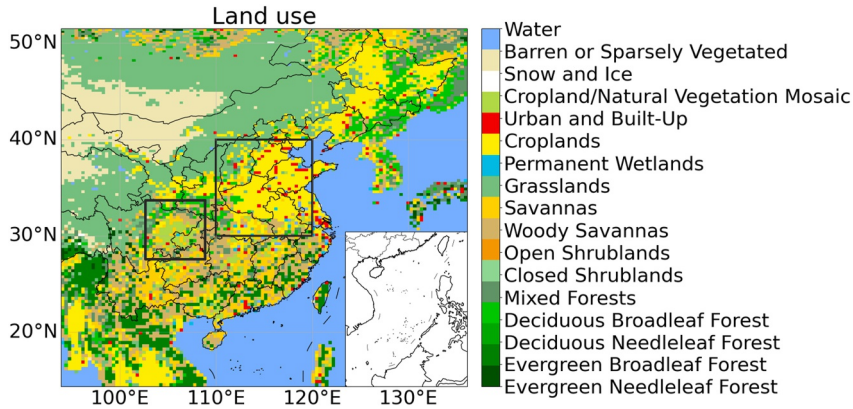

Figure 1. Model domain and land-use classification based on the MODIS MCD12C1 data set for 2020. Colors represent the 17-category IGBP classification scheme, including croplands. The rectangle region highlights the North China Plain, a key agricultural region dominated by winter wheat-summer maize rotations and intensive fertilizer use. The smaller left black line rectangle highlights the Sichuan basin.

Plain (NCP: 30°N–40°N, 110°E−120°E) was selected for focused evaluation. While nesting was not applied, this sub-region allows targeted analysis of NH_3 dynamics in a high-emission zone. The default Modified IGBP-Noah land use data set (circa 2000) was updated to the 2020 MCD12Q1 MODIS product (Friedl & Sulla-Menashe, 2015) to better reflect contemporary cropland distribution in East China, thereby improving the spatial allocation of NH_3 emissions from agricultural activities.

Detailed WRF model parameterization is listed in Table 1, Table 2, and Table S1 in Supporting Information S1. We designed a spatial masking step to ensure that the dynamic emission module applies only to the mainland China region. ERA5 hourly data on pressure levels (Hersbach et al., 2018a) and on single level (Hersbach et al., 2018b) reanalysis data set, which has a spatial resolution of $0.25° \times 0.25°$, was used to drive WRF model as the initial and boundary conditions. The boundary conditions were updated every 6 hr.

The Multi-resolution Emission Inventory for China (MEIC) for the year 2020 (M. Li et al., 2017; B. Zheng et al., 2018) served as the primary emission source for our WRF-CN-Chem experiments. Two simulation experiments are conducted:

1. Offline Run: Agricultural NH_3 emissions are read from the static MEIC inventory. Deposition is calculated by WRF-Chem and removed from the atmosphere, acting as a one-way sink. The land surface (standard Noah-MP) is not affected by deposited nitrogen.
2. Online Run: Agricultural NH_3 emissions are calculated dynamically by Noah-MP-CN. Deposition is calculated by WRF-Chem in the exact same way, but this deposited nitrogen is then fed back into the soil nitrogen pools of Noah-MP-CN. This creates the bidirectional feedback loop where deposition can influence subsequent emissions.

Table 1
The Configuration of Weather Research and Forecasting Parameterization

Physical process	Schemes
Microphysics	Purdue Lin (S.-H. Chen & Sun, 2002)
Cumulus	Grell-Freitas (Grell & Freitas, 2014)
Longwave radiation	RRTMG (Iacono et al., 2008)
Shortwave radiation	RRTMG (Iacono et al., 2008)
Boundary layer	YSU (Hong et al., 2006)
Land surface[a]	Noah-MP (X. Cai et al., 2016; G. Y. Niu et al., 2011)
Surface layer	Revised MM5 (Jiménez et al., 2012)

[a]For the land surface option, we used the original Noah-MP for the Offline experiment and the dynamic nitrogen enhanced Noah-MP-CN for the Online experiment.

MEIC emission inventory includes 31 types of emissions species and different emission sources. We consider industry, power, residential, transportation, and agriculture sources in the Offline experiment. In the Online experiment, agricultural NH_3 emissions are simulated by the dynamic nitrogen cycle module, while non-agricultural NH_3 emissions are still based on the MEIC emission inventory. Both experiments were run for the entire year of 2020. Our analysis confirms that the observed year-to-year variability in monthly temperatures across China remained within the expected range of interannual fluctuations, as quantified by the historical standard deviation. Furthermore, the Niño 3.5 Index (ONI) for 2020 averaged −0.20°C, indicating neutral ENSO conditions with no statistically significant deviation from climatological norms (Figure S2 in Supporting Information S1). The simulation spanned 10 October 2019, to 31 December 2020, with the initial month (1 October–1 November 2019) designated as the spin-up period. All

Table 2
The Configuration of the Noah-MP Model

Physical process	Parameterization schemes
Dynamic vegetation	On, input LAI and FVEG
Canopy stomatal resistance	Ball-Berry
Soil moisture factor for stomatal resistance	Noah
Runoff and groundwater	TOPMODEL with groundwater (Guo-Yue Niu et al., 2007)
Surface layer drag coefficients	M-O
Supercooled liquid water	No iteration (G.-Y. Niu & Yang, 2006)
Frozen soil permeability	Linear effects, are more permeable (G.-Y. Niu & Yang, 2006)
Radiation transfer	Two-stream applied to a vegetated fraction.
Ground snow surface albedo	CLASS
Lower boundary condition of soil temperature	Original Noah
Snow/soil temperature time scheme	Semi-implicit

model configurations—including meteorology, chemistry, and non-agricultural emissions—were identical between experiments, ensuring isolation of the dynamic NH_3 module's impacts.

2.2.4. Fertilization Data and Strategy

Fertilizer application represents the largest anthropogenic source of soil ammonium. Here we adopted the 2020 global crop-specific nitrogen fertilization data set (Wulahati et al., 2023), focusing on five key crops: maize, wheat, rice, vegetables, and fruits. There are 13 nitrogen fertilizer types applied at two depths: surface fertilization (the first 1 cm above the soil surface) and deep fertilization (the top 10 cm below the soil surface). In our fertilization, surface fertilization is conducted 1 cm above the soil surface and at 10 cm under the soil surface for deep fertilization. Fertilization rates for each WRF model grid were calculated by extracting the original data set's rates, multiplying them by cropland area, and normalizing the values by dividing by the grid cell area. Total nitrogen input for each crop was derived by converting all fertilizer types into pure nitrogen equivalents, with aggregated results summarized in Table S2 in Supporting Information S1. This input was then directly allocated to the soil nitrate and ammonium pools. Spatially, high nitrogen inputs for maize, wheat, and vegetables are concentrated in the NCP, while rice and fruit fertilization predominantly occurs in southern China (Figure 2).

Our fertilization strategy accounts for crop rotation practices by aligning with the U.S. Department of Agriculture (USDA) crop calendar for China (Table S3 in Supporting Information S1). We focus on six major crops: spring corn, summer corn, early rice, late tice, spring wheat, and winter wheat. For vegetables and fruits, fertilization occurs continuously throughout the growing season. Fertilization events in the model are distributed across six distinct periods, each spanning 10 days, to simulate staggered application schedules. A detailed description of the fertilizer application schedule is provided in Text S2 in Supporting Information S1.

3. Results

3.1. Annual NH_3 Emission Pattern

We compare NH_3 emissions from our dynamic WRF-CN-Chem model (Online experiment) across the four seasons of 2020 with those from the MEIC inventory, which serves as a widely used, state-of-the-art benchmark rather than an absolute ground truth (Figure 3). The comparison allows us to assess the spatial alignment of major emission regions and highlight key differences in temporal dynamics. Both highlight high emission zones in the NCP and the Sichuan Basin, which is consistent with known major agricultural and industrial activities in these regions. The results demonstrate that the WRF-CN-Chem Online experiment effectively captures these emission hotspots, suggesting that the model's spatial representation of emissions aligns well with the inventory in these key regions.

A seasonal pattern reveals notable differences between the MEIC inventory and the WRF-CN-Chem Online experiment. In winter (DJF), the Online model exhibits lower emissions compared to the MEIC inventory,

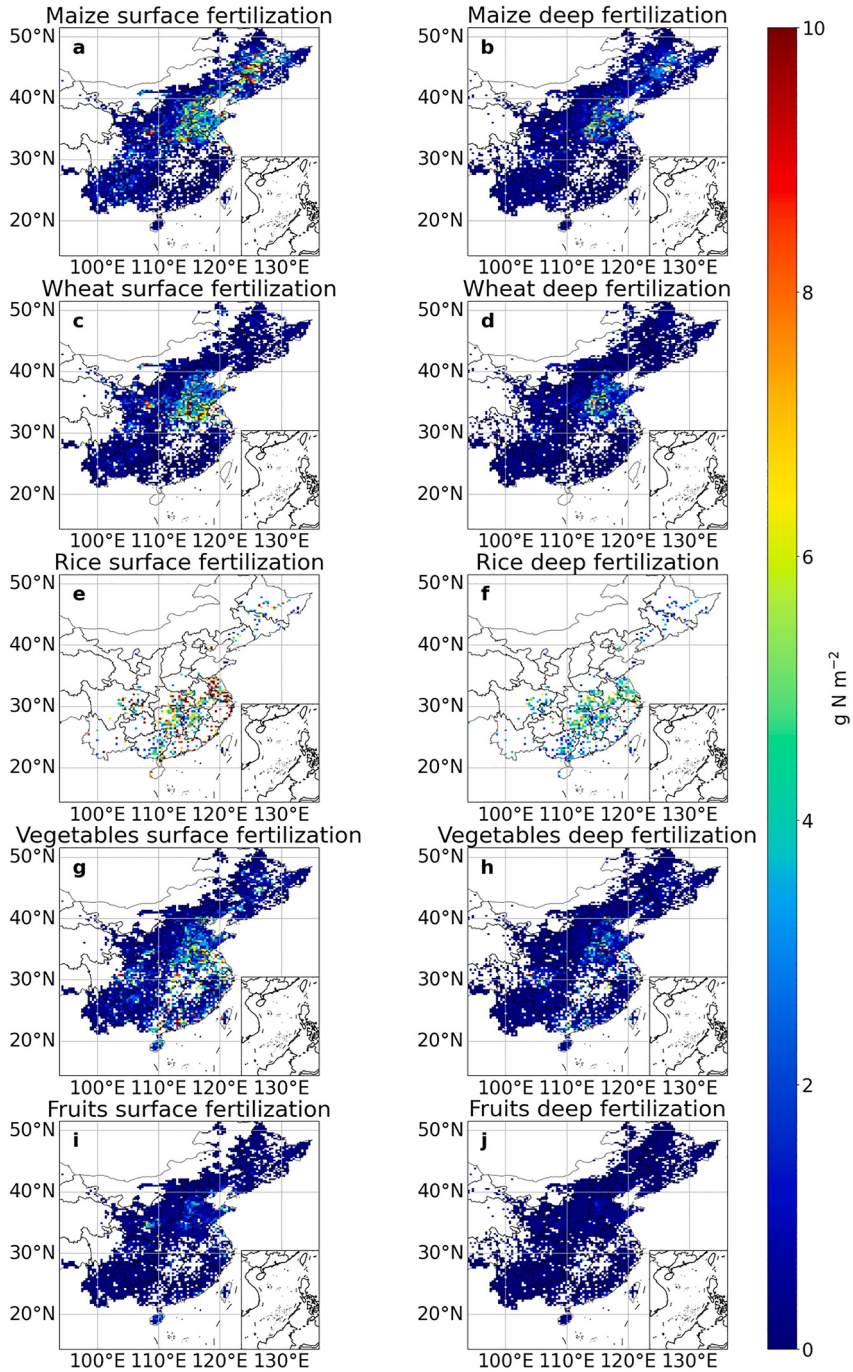

Figure 2. Spatial distribution of annual nitrogen fertilizer application rates (g N m^{-2} yr^{-1}) for five major crop types used in the Online experiment. Surface and deep fertilization indicate 1 cm above the soil layer and 10 cm under the soil layer, respectively.

indicating potential underestimations by the model during colder months. This discrepancy may be attributed to reduced volatilization rates and lower biological activity, which could impact the model's representation of NH_3 emissions. A similar trend is observed in autumn (SON), where the Online experiment underestimates emissions relative to MEIC, potentially reflecting limitations in capturing post-harvest or anthropogenic emission events. In contrast, during spring (MAM) and summer (JJA), the Online and MEIC experiments exhibit similar emission

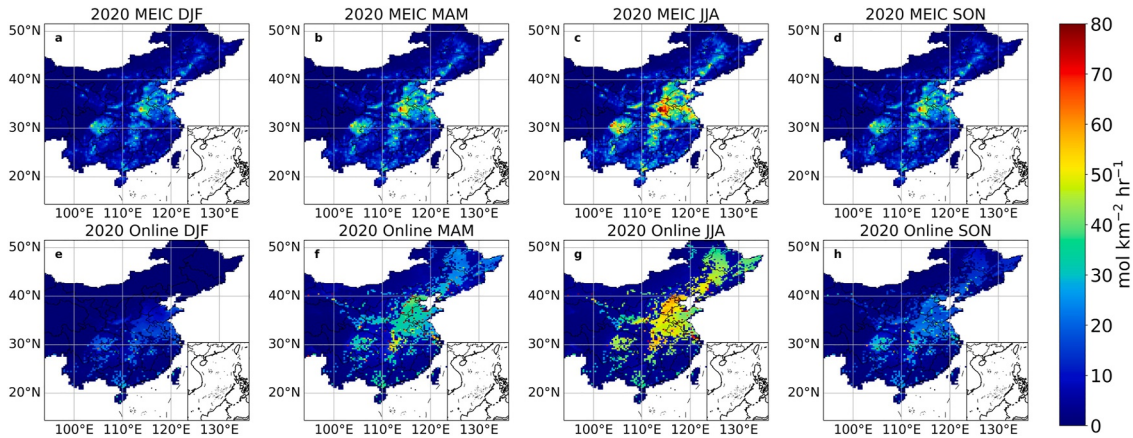

Figure 3. Comparison of seasonal average agricultural ammonia (NH_3) emission fluxes in 2020. (a)–(d) Emissions from the Multi-resolution Emission Inventory for China inventory for winter (DJF), spring (MAM), summer (JJA), and autumn (SON), respectively; (e)–(h) Corresponding emissions simulated by the WRF-CN-Chem Online experiment.

patterns and magnitudes. This suggests that the model's representation of cropland dynamics performs well under conditions of heightened agricultural activity.

The regional mean time series (Figure 4) illustrates that the Offline MEIC experiment does not capture detailed emission variability due to its low temporal resolution. The MEIC emission inventory, constrained to a monthly time resolution, shows a constant emission rate throughout each month. This is because the MEIC inventory applies a fixed 24-hr diurnal pattern to represent daily fluctuations, resulting in limited daily and weekly variability. In contrast, the Online experiment in the WRF-CN-Chem model exhibits higher variability at finer temporal scales, as it dynamically calculates NH_3 emissions at each model timestep. This allows for more

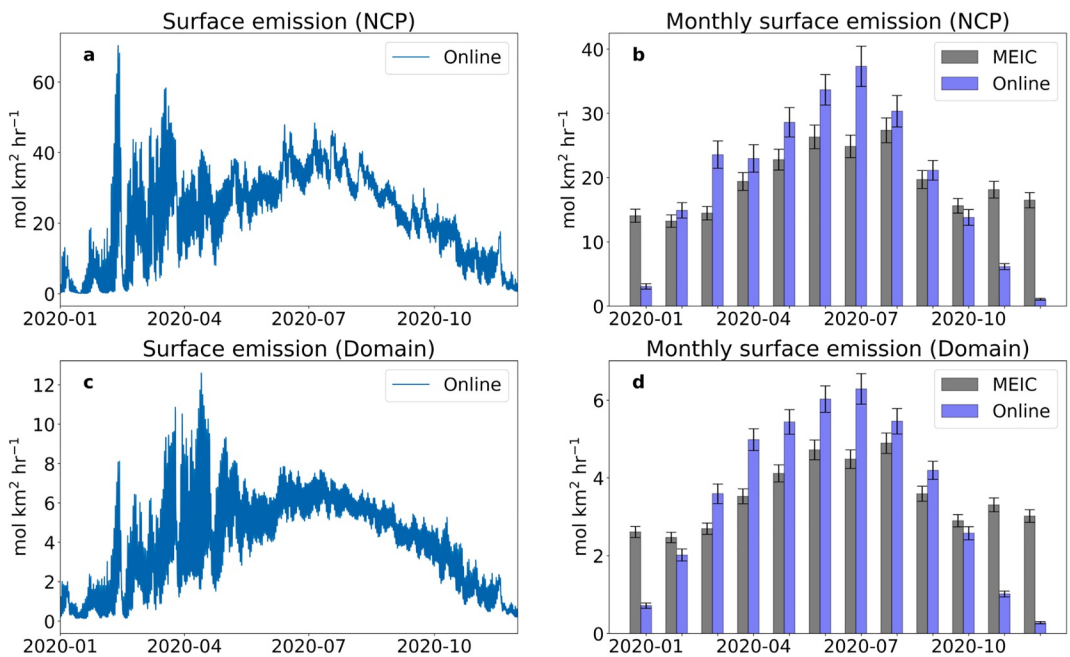

Figure 4. Time series of regional mean ammonia (NH_3) emission fluxes in 2020. (a) High temporal resolution (model timestep) WRF-CN-Chem Online emissions averaged over North China Plain (NCP). (b) Monthly averaged emissions over NCP comparing the Multi-resolution Emission Inventory for China (MEIC) inventory and the Online experiment. (c) High temporal resolution Online emissions averaged over the full model domain. (d) Monthly averaged emissions over the full domain comparing MEIC and the Online experiment. The error band in (a) and (d) indicate ±3 times the standard error of the mean of the spatial average.

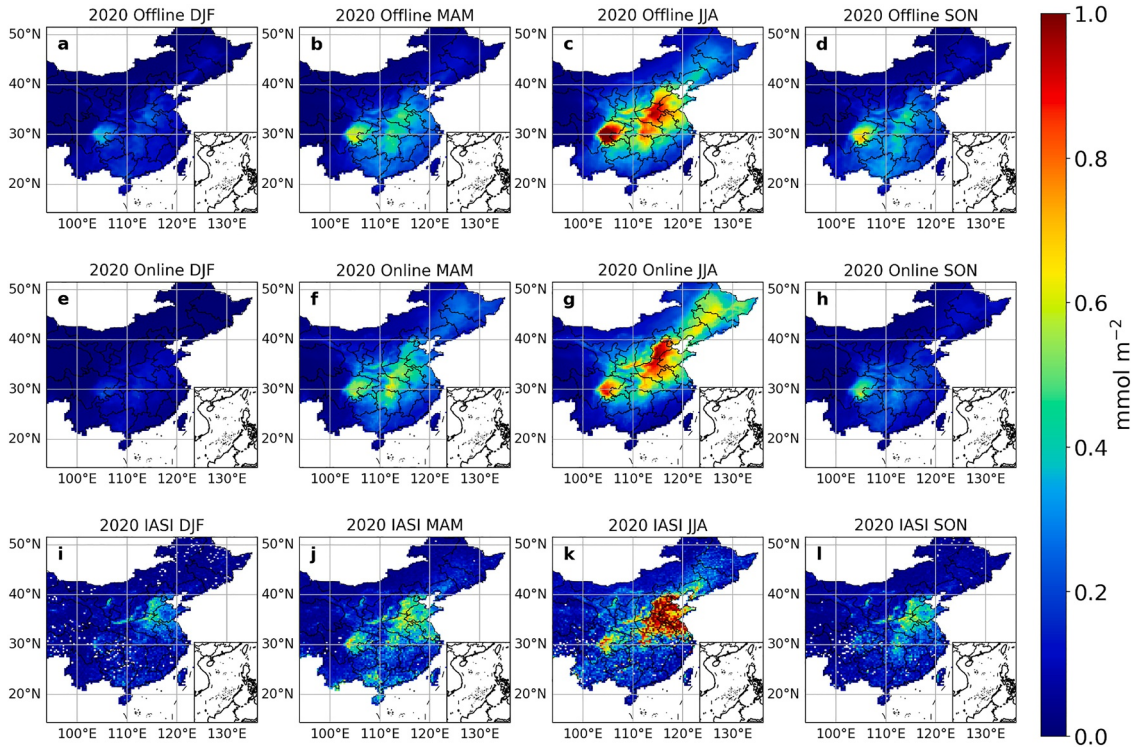

Figure 5. Comparison of seasonal average ammonia total column concentrations in 2020. Panels show results for winter (DJF), spring (MAM), summer (JJA), and autumn (SON) from: (a–d) the Offline experiment (WRF-Chem with Multi-resolution Emission Inventory for China emissions), (e–h) the Online experiment (WRF-CN-Chem with dynamic emissions), and (i–l) IASI satellite observations.

pronounced diurnal cycles and seasonal changes in emissions, resulting in a fluctuating trend that captures short-term variability.

Figure 4b shows the comparison of monthly averaged emissions between the MEIC inventory and the Online experiment for the NCP region. Both experiments effectively represent the annual emission cycle, characterized by a gradual increase in NH_3 emissions from January to July, followed by a decrease from July to December. However, during the winter season, the Online experiment did not maintain high emission levels, with emissions near zero in January, while the MEIC inventory reported a minimum emission rate above 10 mol km^{-2} hr^{-1}. This discrepancy highlights a key difference between the two approaches. While our Online model simulates very low emissions due to its strong temperature dependence, the static MEIC inventory may overestimate NH_3 fluxes during colder months if its monthly scaling factors do not fully account for the sharp reduction in volatilization. This divergence underscores the importance of dynamic modeling for capturing realistic seasonal cycles for temperature-sensitive species like NH_3. In the main domain (Figure 4d), the comparison indicates that the total annual NH_3 emissions from the Online experiment are slightly higher than those of the MEIC inventory. The total NH_3 emissions for year 2020 were 8.55 Tg N for the MEIC inventory, while the Online experiment showed a lower value of 7.88 Tg N. This suggests that the Online experiment, with its dynamic emission calculations, may account for additional emission sources or more responsive emission variability not captured by the fixed monthly emission rates of the MEIC inventory. While MEIC serves as a valuable benchmark for comparison, it is subject to uncertainties in NH_3 magnitude and distribution; our dynamic model may better represent temporal variations under varying land-atmosphere conditions.

3.2. Evaluation of Total Column Concentration

The seasonal NH_3 total column concentrations simulated by the Offline and Online experiments were evaluated against the standard monthly IASI/Metop-B ULB-LATMOS satellite ammonia L3 product (Van Damme et al., 2017) in Figure 5. As indicated by the IASI satellite observations, high-concentration regions are predominantly located in the Sichuan Basin and the NCP, with the NCP being the most intense source region. The

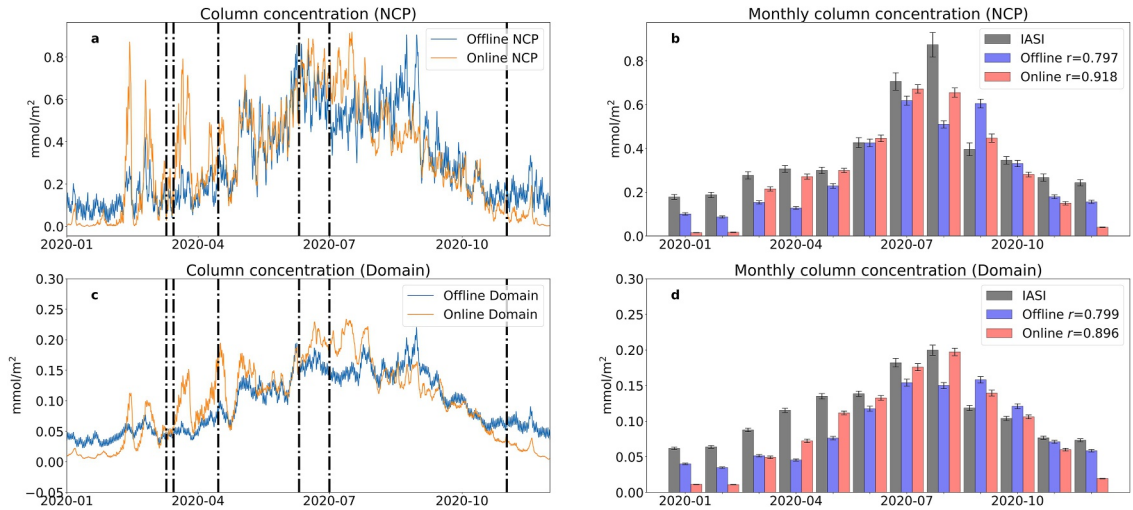

Figure 6. Time series of regional mean ammonia total column concentrations in 2020. (a) High temporal resolution (model timestep) concentrations averaged over North China Plain (NCP) for the Offline and Online experiments. (b) Monthly averaged concentrations over NCP comparing the Offline experiment, Online experiment, and IASI satellite observations. (c) High temporal resolution concentrations averaged over the full model domain for Offline and Online experiments. (d) Monthly averaged concentrations over the full domain comparing Offline, Online, and IASI. Vertical dashed lines in (a) and (c) mark the start dates of fertilization periods in the Online experiment.

NCP exhibits NH_3 column concentrations that often exceed 0.2 mmol m^{-2} NH_3 throughout the year. The Sichuan Basin represents another hotspot but shows a comparable magnitude to the NCP only in spring and summer. Additionally, the South China region, including Guangdong, Guangxi, and Hainan provinces, also exhibits considerable NH_3 levels in spring. The results from both the Offline experiment (Figures 5a–5d) and the Online experiment (Figures 5e–5h) show similar seasonal variability.

However, both experiments exhibit notable spatial biases in the winter and autumn seasons, failing to capture the hotspot over the NCP while overestimating concentrations in the Sichuan Basin. While the exact causes remain uncertain and warrant further investigation, several factors likely contribute to these biases. First, emission inventories like MEIC carry inherent uncertainties due to their relatively coarse spatiotemporal resolution and assumptions regarding winter agricultural activities (e.g., reduced fertilizer application or soil freezing), which may not fully capture localized high emissions in the NCP. Second, our WRF-CN-Chem model, while advancing dynamic bidirectional fluxes, has limitations in simulating winter conditions. As noted in the Discussion section, this could stem from inaccuracies in soil temperature modeling or the omission of key variables such as soil pH, moisture, and wind speed, which critically influence NH_3 volatilization rates under cold and dry conditions. Additionally, broader systematic errors in the WRF-Chem framework (e.g., chemical mechanisms) could play a role. Finally, potential biases in the satellite product itself should be considered. As noted by Van Damme et al. (2014), satellite retrieval algorithms can sometimes exhibit biases in regions with high aerosol loadings or thermal contrast issues, which could contribute to the apparent severity of the model-observation discrepancy.

Notably, both approaches successfully capture the NCP hotspot in summer, when warmer temperatures and peak agricultural activity align well with model dynamics. This suggests that the observed biases are likely seasonally specific process limitations rather than fundamental errors in the coupling framework.

The regional mean time series of column concentration (Figure 6) reveals consistent seasonal trends in both experiments, with NH_3 concentrations gradually increasing from winter through summer and subsequently decreasing from summer to winter. This pattern reflects typical agricultural practices, such as fertilizer application, and temperature-driven volatilization processes that enhance NH_3 emissions in warmer months. Online experiment demonstrates higher variability within shorter time periods due to the dynamic emission process being conducted at each model timestep. This allows for more detailed representation of diurnal and seasonal changes in emissions. In the winter season, the Online experiment shows notably lower total column concentrations compared to the Offline experiment, consistent with reduced NH_3 emissions observed during this period. This may be attributed to the model's representation of temperature-dependent processes that influence NH_3

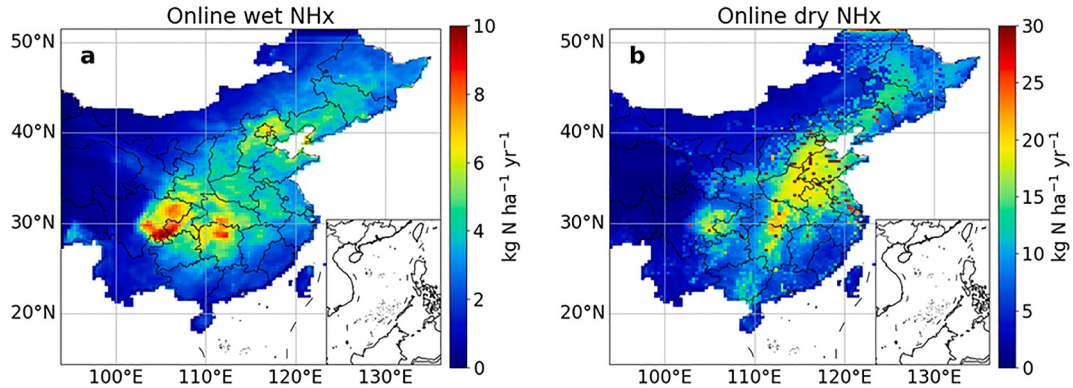

Figure 7. Spatial distribution of NH_x deposition fluxes across the model domain in 2020. (a) NH_x wet deposition. (b) NH_x dry deposition.

volatilization. The Offline experiment, constrained by a fixed monthly emission pattern, lacks the capability to represent these finer temporal fluctuations.

Quantitative comparison with IASI data (Figures 6b and 6d) highlights the Online experiment's superior performance. The correlation coefficient for the Online experiment in the NCP is 0.92 ($p < 0.05$), substantially higher than the 0.80 for the Offline experiment. Similarly, in the main domain, the Online experiment achieves a correlation of 0.95 compared to 0.78 for the Offline experiment. This suggests that the dynamic emission approach used in the Online experiment better represents the actual temporal variability of NH_3 concentrations, aligning more closely with observations. The enhanced performance of the Online experiment is attributed to its ability to simulate NH_3 emission variability due to agricultural activities and environmental conditions, providing a more realistic depiction of diurnal and seasonal fluctuations. The higher variability and the presence of concentration spikes starting from March highlight the impact of fertilization activities and other emissions linked to agricultural practices. The Offline experiment, by contrast, shows less fluctuations that are driven by the monthly MEIC inventory, failing to capture these short-term variations.

3.3. Atmosphere Deposition and Its Impact on Land System

Atmospheric deposition is a crucial component of the nitrogen cycle and a key variable in our model. We incorporated additional pollutant gases, such as nitrogen dioxide (NO_2) and sulfur dioxide (SO_2), from the MEIC Inventory. Some of these gases are acidic species that can react with ammonia (NH_3) in the atmosphere to form secondary inorganic aerosols. As denoted by (Lachatre et al., 2019), declining acid gas emissions can lead to increased atmospheric NH_3 due to reduced aerosol formation.

Through dry and wet deposition processes, NH_3 and ammonium (NH_4^+) are deposited onto the land surface, contributing to the ammonium pool. Even though WRF-CN-Chem the overestimates the total inorganic nitrogen deposition (Text S3 and Figure S3 in Supporting Information S1), in 2020, the estimated total dry NH_x deposition flux was 6.22 Tg N yr^{-1} (Figure 7b), which is close to the annual average of 6.8 ± 0.6 Tg N yr^{-1} for 2011–2015 reported by Yu et al. (2019). Our Online experiment showed a lower value for wet NH_x deposition at 2.23 Tg N yr^{-1} (Figure 7a) compared to their reported 5.7 ± 0.5 Tg N yr^{-1}. This discrepancy may reflect the combined effects of rising anthropogenic NO_x emissions since 2010 (B. Zheng et al., 2018), which enhance atmospheric oxidation capacity and aerosol formation, and biases in the WRF-Chem wet deposition scheme. Figure S4 in Supporting Information S1 indicates that the WRF model overestimates total precipitation throughout the year, suggesting there should be more wet NH_x deposition than simulated. The bias in simulated wet deposition can be attributed to the selection of the wet deposition scheme in the WRF-Chem model. Different schemes in WRF-Chem employ various chemical mechanisms, which may lead to significant discrepancies in the results.

The soil nitrogen pool receives supplemental nitrogen through atmospheric deposition, which can enhance NH_3 emissions via volatilization. To evaluate the influence of the bidirectional exchange of NH_3 in the model, we designed a sensitivity experiment that excludes dynamic nitrogen deposition to the land surface. Focusing solely

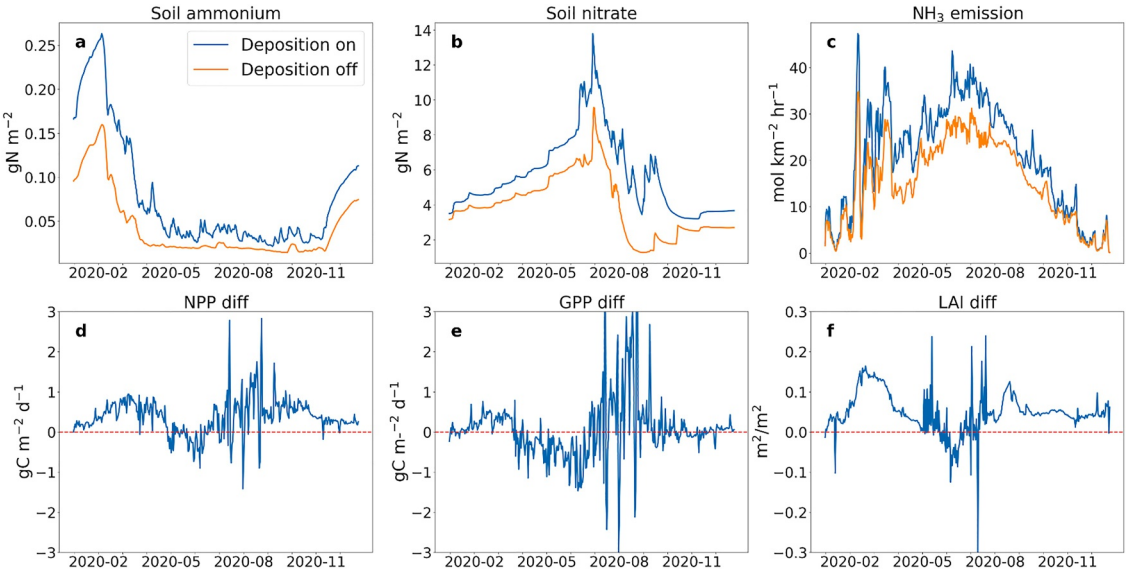

Figure 8. Effect of atmospheric nitrogen deposition (enabled vs. disabled) on key variables simulated by the Online experiment, averaged over North China Plain for 2020. (a) Soil ammonium pool. (b) Soil nitrate pool., (c) Daily NH_3 emission. (d)–(f) Daily difference ("On" minus "Off") for: (d) net primary productivity, (e) gross primary productivity, and (f) leaf area index.

on the NCP, we assessed changes in soil ammonium (NH_4^+) and nitrate (NO_3^-) concentrations, ammonia volatilization, and variables related to land productivity (Figure 8).

Deactivating nitrogen deposition significantly reduced both soil NH_4^+ and NO_3^- pools in the NCP (Figures 8a and 8b). Total NH_3 emissions decreased by 41% to 4.64 Tg N yr^{-1} compared to simulations with active nitrogen deposition. The impact of this reduction is evident in related processes, as shown by the results for net primary productivity (NPP), gross primary productivity (GPP), and leaf area index (LAI). Specifically, in the NCP region, deactivating nitrogen deposition led to an average annual decrease in NPP of 0.38 g C m^{-2} d^{-1}, while GPP and LAI decreased by 0.07 g C m^{-2} d^{-1} and 0.05 m^2 m^{-2}, respectively.

The interaction between the land surface system and nitrogen deposition is complex yet critical. The land surface system encompasses physical and biological processes—including soil nutrient pools and plant cover—that interact with atmospheric nitrogen inputs. Nitrogen deposition provides an external source of nitrogen that can be assimilated by vegetation and incorporated into the soil, affecting both plant growth and soil fertility. When nitrogen deposition is active, it supplies additional nitrogen that boosts the nutrient pool, enabling higher rates of photosynthesis and plant productivity, as reflected by increases in NPP, GPP, and LAI. This interaction fosters a positive feedback loop, where plants with sufficient nitrogen support more robust growth and carbon–nitrogen uptake. Conversely, when nitrogen deposition is deactivated, the absence of this nutrient input disrupts the balance within the land system. Plants may experience nutrient limitations, leading to reduced productivity, as evidenced by declines in NPP and GPP. The reduced nitrogen availability in the soil also affects microbial processes that facilitate nitrogen cycling, further impacting plant growth conditions. M. Liu et al. (2022) found that a 30% reduction in NO_x emissions leads to 12% reduction in total nitrogen deposition from domestic sources, reducing the net ecosystem production by 11.2 Tg C yr^{-1}. They conclude that decreased nitrogen deposition impairs plant nitrogen uptake for growth and reduces NPP due to nitrogen limitation. Our experiment reveals that nitrogen deposition is crucial not only as a source of nitrogen for the soil pool but also for maintaining ecosystem functions through its interaction with the land system. The absence of dynamic deposition resulted in a 2.25 Tg C yr^{-1} (at a 95% confidence interval of [2.21, 2.28] Tg C yr^{-1}) reduction of NPP over the whole domain (eastern China), underscoring its necessity for maintaining agricultural and ecological productivity.

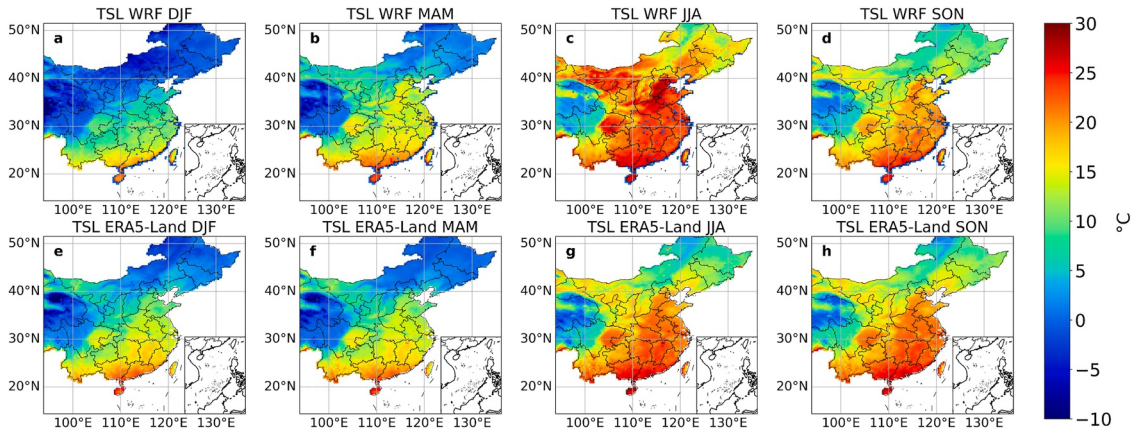

Figure 9. Comparison of seasonal average depth-weighted soil column temperature in 2020 between the WRF-CN-Chem simulation and the ERA5-Land reanalysis data set. (a–d) WRF-CN-Chem results for winter (DJF), spring (MAM), summer (JJA), and autumn (SON), respectively, weighted across model soil layers (depths: 10, 30, 60, 100 cm). (e–h) Corresponding ERA5-Land data for the same seasons, weighted across data set layers (depths: 7, 21, 72, 189 cm).

4. Discussion

4.1. Uncertainties of Factors When Estimating NH_3 Emission Magnitude

Our dynamic NH_3 emission and nitrogen deposition model demonstrates robust performance in simulating the land-atmosphere nitrogen cycling. We also evaluated our WRF-CN-Chem model's performance on simulating near surface meteorological filed (2 m air temperature, 2 m relative humidity, 10 m wind speed as well as precipitation), showing reasonable results (see Text S4 and Figures S5–S6 in Supporting Information S1 for a full evaluation). However, uncertainties exist in our strategy. Currently, soil temperature serves as the primary driving factor in estimating NH_3 emissions in our study. Figure 9 compares the spatial pattern of depth-weighted soil column temperatures simulated by WRF-CN-Chem against the ERA5-Land data set (Muñoz-Sabater et al., 2021). Generally, WRF-CN-Chem performed well in simulating the annual cycle and magnitude of soil temperature, with high spatial correlation coefficients across seasons (0.93 in winter, 0.96 in spring, 0.84 in summer, and 0.95 in autumn; $p < 0.5$). This strong agreement between modeled and observed data supports the reliability of the dynamic NH_3 emission model. Further comparisons for 2 m air temperature, surface skin temperature and precipitation between WRF-CN-Chem and ERA5 are shown in Figures S7–S8 in Supporting Information S1.

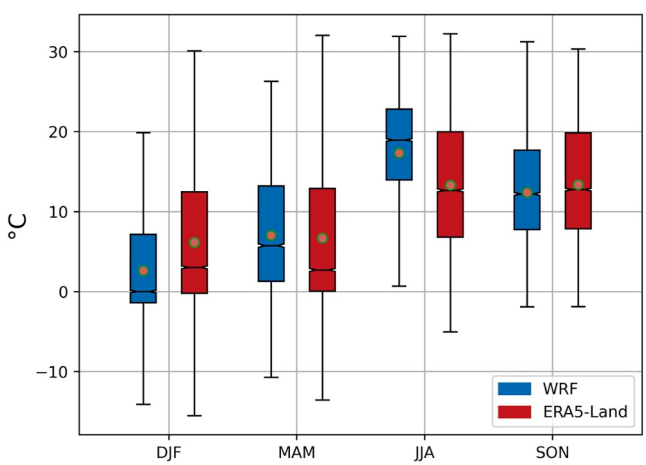

Figure 10. Boxplot comparison of domain-averaged, depth-weighted soil temperatures for each season in 2020 between WRF-CN-Chem and ERA5-Land. Boxes show the interquartile range (25th–75th percentiles), the horizontal line within the box is the median, and the green circled red dot represents the mean.

Comparing the spatially averaged soil temperature in four seasons from WRF-CN-Chem with ERA5-Land (Figure 10), winter and autumn temperatures are underestimated by 3.54°C and 0.98°C, respectively, potentially contributing to reduced NH_3 emissions and total column concentration in the Online experiment. These discrepancies may arise from Noah-MP's configuration, where choices in dynamic vegetation, soil moisture factor, and radiation transfer schemes influence the accuracy of modeled soil temperature. While our temperature-dependent parameterization provides a foundational representation, it omits key physiochemical drivers such as soil moisture, humidity, and pH, which can govern NH_3 fluxes from wet or drying surfaces (Jiang et al., 2024). Further enhancements to Noah-MP-CN will aim to include these factors for improved dynamism.

4.2. Soil Nitrogen Pool and Mineralization Process

Soil nitrate and organic nitrogen pools are initialized with prescribed parameterization. Obtaining a stable and accurate nitrogen pool needs a multi-year spin-up period in the Noah-MP model. Accurate modeling of biogeochemical cycles in land surface models continues to rely on high-resolution soil data sets that include detailed representations of land use and land

cover, soil properties, and soil nutrient distribution. More realistic soil nitrogen stock input could further reduce initialization errors.

The mineralization process is influenced by soil microbial processes and properties (Guo et al., 2019). However, Noah-MP lacks explicit microbial process representations, limiting its ability to resolve nitrogen transformation kinetics. In this study, we modified the mineralization process—specifically, allocating 20% of mineralized nitrogen to the soil ammonium pool—enhanced NH_3 emission simulations. This empirical adjustment, while effective in aligning modeled NH_3 patterns with observations in eastern China, introduces uncertainties due to sparse experimental data on ammonium-to-nitrate conversion rates. Advancing biogeochemical modules in future Noah-MP-CN development to explicitly incorporate microbial dynamics—such as enhanced representations of soil total ammoniacal nitrogen partitioning, mineralization, nitrification, and diffusion processes—will address this gap, building on process-based approaches demonstrated in recent models (Fung et al., 2022; Jiang et al., 2024; Vira et al., 2022).

4.3. Agriculture Activities

Fertilization is the major source of soil nitrogen pools, which can be conducted in various formations regarding the content of synthetic fertilizer type, the depth of fertilization, and fertilization period. Although fertilizer deep placement can reduce total soil gaseous nitrogen compound emissions by 84% (Song et al., 2024), it is not yet a common practice in NCP. In our model, therefore, fertilization is conducted within the top 10 cm of the soil. The nitrate-to-ammonium ratio, which is set to 0.5 here, also impacts emissions: increasing nitrate fertilizer lowers NH_3 emissions but increase N_2O emissions (Y. Zhang et al., 2016).

China's diverse agricultural landscape, dominated by smallholder farms with variable fertilization schedules (Chenchen Ren et al., 2021) makes it impractical to implement a uniform fertilization parameterization in the model. In addition, the specific crop planting periods and strategies for fertilization and irrigation vary from year to year. Although the crop calendar serves as the primary reference, it necessitates thorough field investigations conducted at a high spatial resolution for accurate representation. For instance, the maize–wheat rotation system in the NCP drives biannual emission peaks (Y. Cai et al., 2013). Future integration with the Noah-MP-Crop model (X. Liu et al., 2016) will enable species-specific simulations (e.g., soybean, corn, rice) and dynamic crop rotation schemes, better aligning the model with real-world practices.

5. Conclusions

This study advances regional nitrogen cycle modeling by coupling the Noah-MP-CN LSM with the WRF-Chem atmospheric chemistry framework. Our key achievement lies in the development of a state-of-the-art dynamic NH_3 emission and nitrogen deposition module, enabling bidirectional land-atmosphere exchange of reduced nitrogen. Unlike static emission inventories, our approach integrates a fertilization data set encompassing five crop types, 13 fertilizer compounds, and non-agricultural NH_3 sources, significantly improving the representation of emission processes tied to agricultural practices. A crop calendar-based fertilization routine further refines temporal accuracy. Compared with other bidirectional model with sperate pre-processing tool (e.g., EPIC's detailed crop management simulations), this model provides a more seamless, flexible integration entirely within the WRF framework, eliminating the need for external models or additional preprocessing steps. This unified structure enhances computational efficiency and facilitates easier application to diverse regional scales.

Sensitivity experiments demonstrate that the Online experiment captures seasonal trends and magnitudes of NH_3 fluxes and total column concentrations with high fidelity. The model shows strong spatial and temporal agreement with MEIC inventories and accurately identifies emission hotspots in NCP and the Sichuan Basin, as validated against IASI satellite retrievals. Across the simulation domain (eastern China), the Online experiment estimates total NH_3 emissions at 7.88 Tg N yr^{-1}, with 41% attributed to re-emission from deposited nitrogen. Crucially, excluding dynamic nitrogen deposition reduces NPP by 2.25 Tg C yr^{-1}, underscoring deposition's vital role in sustaining ecosystem function.

By resolving bidirectional nitrogen exchange and deposition feedbacks, this work reduces uncertainties in regional biogeochemical simulations. Our framework provides a foundation for integrating chemical and land surface models, offering insights critical for sustainable agricultural management and pollution mitigation strategies.

Conflict of Interest

The authors declare no conflicts of interest relevant to this study.

Data Availability Statement

The WRF-Chem version 4.1.2 is from Skamarock et al. (2019). The fertilizer data sets are provided by the National Tibetan Plateau/Third Pole Environment Data Center (Wulahati et al., 2023). The ERA5 reanalysis data set is from Copernicus Climate Change Service (C3S) Climate Data Store (Hersbach et al., 2018a, Hersbach et al., 2018b). The IASI NH3 total column concentration data can be downloaded from Van Damme et al. (2014). The MEIC inventory data sets is from M. Li et al. (2017). The MCD12C1 MODIS/Terra + Aqua Land Cover data set is from Friedl and Sulla-Menashe (2015). The WRF-CN-Chem's output and post-processing code can be found at Cao et al. (2025).

Acknowledgments
This work is supported by the National Key Research and Development Program of China (2023YFF0805501) and the National Natural Science Foundation of China (42375165). The authors would like to thank Mr. Aoxuan Chen and Ms. Zilu Zhang for their help in designing the model structure.

References

Asaadi, A., & Arora, V. K. (2021). Implementation of nitrogen cycle in the CLASSIC land model. *Biogeosciences*, *18*(2), 669–706. https://doi.org/10.5194/bg-18-669-2021

Bash, J., Cooter, E., Dennis, R., Walker, J., & Pleim, J. (2013). Evaluation of a regional air-quality model with bidirectional NH 3 exchange coupled to an agroecosystem model. *Biogeosciences*, *10*(3), 1635–1645. https://doi.org/10.5194/bg-10-1635-2013

Bhautmage, U. P., Fung, J. C. H., Pleim, J., & Wong, M. M. F. (2022). Development and evaluation of a new urban parameterization in the weather research and forecasting (WRF) model. *Journal of Geophysical Research: Atmospheres*, *127*(16), e2021JD036338. https://doi.org/10.1029/2021jd036338

Binkowski, F. S., & Shankar, U. (1995). The regional particulate matter model: 1. Model description and preliminary results. *Journal of Geophysical Research*, *100*(D12), 26191–26209. https://doi.org/10.1029/95JD02093

Cai, X., Cao, Y., Zhang, G., Liang, J., Zheng, H., Li, K., et al. (2024). Influence of terrestrial nitrogen dynamics on mesoscale near-surface meteorological fields. *Journal of Geophysical Research: Atmospheres*, *129*(14), e2023JD040168. https://doi.org/10.1029/2023JD040168

Cai, X., Yang, Z. L., Fisher, J. B., Zhang, X., Barlage, M., & Chen, F. (2016). Integration of nitrogen dynamics into the Noah-MP land surface model v1.1 for climate and environmental predictions. *Geoscientific Model Development*, *9*(1), 1–15. https://doi.org/10.5194/gmd-9-1-2016

Cai, Y., Ding, W., & Luo, J. (2013). Nitrous oxide emissions from Chinese maize–wheat rotation systems: A 3-year field measurement. *Atmospheric Environment*, *65*, 112–122. https://doi.org/10.1016/j.atmosenv.2012.10.038

Cao, Y., Ren, C., Zhang, H., Wei, Z., Guo, Y., & Cai, X. (2025). Dynamic modeling of ammonia emissions and nitrogen deposition via online coupling of WRF-Chem and Noah-MP-CN. *Retrieved from*. https://doi.org/10.5281/zenodo.15322239

Chen, S.-H., & Sun, W.-Y. (2002). A one-dimensional time dependent cloud model. *Journal of the Meteorological Society of Japan. Series II*, *80*(1), 99–118. https://doi.org/10.2151/jmsj.80.99

Chen, Y., Zhang, L., Henze, D. K., Zhao, Y., Lu, X., Winiwarter, W., et al. (2021). Interannual variation of reactive nitrogen emissions and their impacts on PM2. 5 air pollution in China during 2005–2015. *Environmental Research Letters*, *16*(12), 125004. https://doi.org/10.1088/1748-9326/ac3695

Cornell, S., Jickells, T., Cape, J., Rowland, A., & Duce, R. (2003). Organic nitrogen deposition on land and coastal environments: A review of methods and data. *Atmospheric Environment*, *37*(16), 2173–2191. https://doi.org/10.1016/S1352-2310(03)00133-X

Davies-Barnard, T., Meyerholt, J., Zaehle, S., Friedlingstein, P., Brovkin, V., Fan, Y., et al. (2020). Nitrogen cycling in CMIP6 land surface models: Progress and limitations. *Biogeosciences*, *17*(20), 5129–5148. https://doi.org/10.5194/bg-17-5129-2020

Easter, R. C., Ghan, S. J., Zhang, Y., Saylor, R. D., Chapman, E. G., Laulainen, N. S., et al. (2004). MIRAGE: Model description and evaluation of aerosols and trace gases. *Journal of Geophysical Research*, *109*(D20). https://doi.org/10.1029/2004JD004571

Elrys, A. S., Ali, A., Zhang, H., Cheng, Y., Zhang, J., Cai, Z. C., et al. (2021). Patterns and drivers of global gross nitrogen mineralization in soils. *Global Change Biology*, *27*(22), 5950–5962. https://doi.org/10.1111/gcb.15851

Erisman, J. W., Sutton, M. A., Galloway, J., Klimont, Z., & Winiwarter, W. (2008). How a century of ammonia synthesis changed the world. *Nature Geoscience*, *1*(10), 636–639. https://doi.org/10.1038/ngeo325

Friedl, M., & Sulla-Menashe, D. (2015). MCD12C1 MODIS/Terra+ aqua land cover type yearly L3 global 0.05 deg CMG V006. https://doi.org/10.5067/MODIS/MCD12C1.006

Fu, X., Wang, S., Ran, L., Pleim, J., Cooter, E., Bash, J., et al. (2015). Estimating NH 3 emissions from agricultural fertilizer application in China using the bi-directional CMAQ model coupled to an agro-ecosystem model. *Atmospheric Chemistry and Physics*, *15*(12), 6637–6649. https://doi.org/10.5194/acp-15-6637-2015

Fu, X., Wang, S., Xing, J., Zhang, X., Wang, T., & Hao, J. (2017). Increasing ammonia concentrations reduce the effectiveness of particle pollution control achieved via SO2 and NO X emissions reduction in east China. *Environmental Science and Technology Letters*, *4*(6), 221–227. https://doi.org/10.1021/acs.estlett.7b00143

Fung, K. M., Val Martin, M., & Tai, A. P. (2022). Modeling the interinfluence of fertilizer-induced NH 3 emission, nitrogen deposition, and aerosol radiative effects using modified CESM2. *Biogeosciences*, *19*(6), 1635–1655. https://doi.org/10.5194/bg-19-1635-2022

Gerber, S., Hedin, L. O., Oppenheimer, M., Pacala, S. W., & Shevliakova, E. (2010). Nitrogen cycling and feedbacks in a global dynamic land model. *Global Biogeochemical Cycles*, *24*(1), GB1001. https://doi.org/10.1029/2008GB003336

Grell, G. A., & Dévényi, D. (2002). A generalized approach to parameterizing convection combining ensemble and data assimilation techniques. *Geophysical Research Letters*, *29*(14), 38-31–34. https://doi.org/10.1029/2002GL015311

Grell, G. A., & Freitas, S. R. (2014). A scale and aerosol aware stochastic convective parameterization for weather and air quality modeling. *Atmospheric Chemistry and Physics*, *14*(10), 5233–5250. https://doi.org/10.5194/acp-14-5233-2014

Gu, B., Zhang, L., Van Dingenen, R., Vieno, M., Van Grinsven, H. J., Zhang, X., et al. (2021). Abating ammonia is more cost-effective than nitrogen oxides for mitigating PM2. 5 air pollution. *Science*, *374*(6568), 758–762. https://doi.org/10.1126/science.abf8623

Guo, Z., Han, J., Li, J., Xu, Y., & Wang, X. (2019). Effects of long-term fertilization on soil organic carbon mineralization and microbial community structure. *PLoS One*, *14*(1), e0211163. https://doi.org/10.1371/journal.pone.0211163

Han, W.-J., Cao, J.-Y., Liu, J.-L., Jiang, J., & Ni, J. (2019). Impacts of nitrogen deposition on terrestrial plant diversity: A meta-analysis in China. *Journal of Plant Ecology*, *12*(6), 1025–1033. https://doi.org/10.1093/jpe/rtz036

Hersbach, H., Bell, B., Berrisford, P., Biavati, G., Horányi, A., Muñoz Sabater, J., et al. (2018a). *ERA5 hourly data on pressure levels from 1979 to present*. Retrieved from. https://doi.org/10.24381/cds.bd0915c6

Hersbach, H., Bell, B., Berrisford, P., Biavati, G., Horányi, A., Muñoz Sabater, J., et al. (2018b). ERA5 hourly data on single levels from 1979 to present. https://doi.org/10.24381/cds.adbb2d47

Hong, S.-Y., Noh, Y., & Dudhia, J. (2006). A new vertical diffusion package with an explicit treatment of entrainment processes. *Monthly Weather Review*, *134*(9), 2318–2341. https://doi.org/10.1175/MWR3199.1

Huang, X., Song, Y., Li, M., Li, J., Huo, Q., Cai, X., et al. (2012). A high-resolution ammonia emission inventory in China. *Global Biogeochemical Cycles*, *26*(1), GB1030. https://doi.org/10.1029/2011GB004161

Iacono, M. J., Delamere, J. S., Mlawer, E. J., Shephard, M. W., Clough, S. A., & Collins, W. D. (2008). Radiative forcing by long-lived greenhouse gases: Calculations with the AER radiative transfer models. *Journal of Geophysical Research*, *113*(D13), D13103. https://doi.org/10.1029/2008JD009944

Jiang, J., Stevenson, D. S., & Sutton, M. A. J. E. (2024). A dynamical process-based model AMmonia. *CLIMate v1. 0 (AMCLIM v1. 0) for quantifying global agricultural ammonia emissions–Part 1: Land module for simulating emissions from synthetic fertilizer use*, *2024*, 1–59. https://doi.org/10.5194/egusphere-2024-962

Jiménez, P. A., Dudhia, J., González-Rouco, J. F., Navarro, J., Montávez, J. P., & García-Bustamante, E. (2012). A revised scheme for the WRF surface layer formulation. *Monthly Weather Review*, *140*(3), 898–918. https://doi.org/10.1175/MWR-D-11-00056.1

Kang, Y., Liu, M., Song, Y., Huang, X., Yao, H., Cai, X., et al. (2016). High-resolution ammonia emissions inventories in China from 1980 to 2012. *Atmospheric Chemistry and Physics*, *16*(4), 2043–2058. https://doi.org/10.5194/acp-16-2043-2016

Lachatre, M., Fortems-Cheiney, A., Foret, G., Siour, G., Dufour, G., Clarisse, L., et al. (2019). The unintended consequence of SO 2 and NO 2 regulations over China: Increase of ammonia levels and impact on PM 2.5 concentrations. *Atmospheric Chemistry and Physics*, *19*(10), 6701–6716. https://doi.org/10.5194/acp-19-6701-2019

Li, H., Wang, L., Peng, Y., Zhang, S., Lv, S., Li, J., et al. (2021). Film mulching, residue retention and N fertilization affect ammonia volatilization through soil labile N and C pools. *Agriculture, Ecosystems & Environment*, *308*, 107272. https://doi.org/10.1016/j.agee.2020.107272

Li, M., Liu, H., Geng, G., Hong, C., Liu, F., Song, Y., et al. (2017). Anthropogenic emission inventories in China: A review. *National Science Review*, *4*(6), 834–866. https://doi.org/10.1093/nsr/nwx150

Liu, M., Shang, F., Lu, X., Huang, X., Song, Y., Liu, B., et al. (2022). Unexpected response of nitrogen deposition to nitrogen oxide controls and implications for land carbon sink. *Nature Communications*, *13*(1), 3126. https://doi.org/10.1038/s41467-022-30854-y

Liu, X., Chen, F., Barlage, M., Zhou, G., & Niyogi, D. (2016). Noah-MP-Crop: Introducing dynamic crop growth in the Noah-MP land surface model. *Journal of Geophysical Research: Atmospheres*, *121*(23), 13953–913972. https://doi.org/10.1002/2016JD025597

Ma, R., Zou, J., Han, Z., Yu, K., Wu, S., Li, Z., et al. (2021). Global soil-derived ammonia emissions from agricultural nitrogen fertilizer application: A refinement based on regional and crop-specific emission factors. *Global Change Biology*, *27*(4), 855–867. https://doi.org/10.1111/gcb.15437

Martínez-Dalmau, J., Berbel, J., & Ordóñez-Fernández, R. (2021). Nitrogen fertilization. A review of the risks associated with the inefficiency of its use and policy responses. *Sustainability*, *13*(10), 5625. https://doi.org/10.3390/su13105625

Muñoz-Sabater, J., Dutra, E., Agustí-Panareda, A., Albergel, C., Arduini, G., Balsamo, G., et al. (2021). ERA5-Land: A state-of-the-art global reanalysis dataset for land applications. *Earth System Science Data*, *13*(9), 4349–4383. https://doi.org/10.5194/essd-13-4349-2021

Niu, G.-Y., & Yang, Z.-L. (2006). Effects of frozen soil on snowmelt runoff and soil water storage at a continental scale. *Journal of Hydrometeorology*, *7*(5), 937–952. https://doi.org/10.1175/JHM538.1

Niu, G. Y., Yang, Z. L., Dickinson, R. E., Gulden, L. E., & Su, H. (2007). Development of a simple groundwater model for use in climate models and evaluation with Gravity Recovery and Climate Experiment data. *Journal of Geophysical Research*, *112*(D7), D07103. https://doi.org/10.1029/2006JD007522

Niu, G. Y., Yang, Z. L., Mitchell, K. E., Chen, F., Ek, M. B., Barlage, M., et al. (2011). The community Noah land surface model with multiparameterization options (Noah-MP): 1. Model description and evaluation with local-scale measurements. *Journal of Geophysical Research*, *116*(D12), D12109. https://doi.org/10.1029/2010JD015139

Paulot, F., Jacob, D. J., Pinder, R., Bash, J., Travis, K., & Henze, D. (2014). Ammonia emissions in the United States, European Union, and China derived by high-resolution inversion of ammonium wet deposition data: Interpretation with a new agricultural emissions inventory (MASAGE_NH3). *Journal of Geophysical Research: Atmospheres*, *119*(7), 4343–4364. https://doi.org/10.1002/2013JD021130

Reay, D. S., Dentener, F., Smith, P., Grace, J., & Feely, R. A. (2008). Global nitrogen deposition and carbon sinks. *Nature Geoscience*, *1*(7), 430–437. https://doi.org/10.1038/ngeo230

Ren, C., Huang, X., Liu, T., Song, Y., Wen, Z., Liu, X., et al. (2023). A dynamic ammonia emission model and the online coupling with WRF–Chem (WRF–SoilN–Chem v1. 0): Development and regional evaluation in China. *Geoscientific Model Development*, *16*(6), 1641–1659. https://doi.org/10.5194/gmd-16-1641-2023

Ren, C., Jin, S., Wu, Y., Zhang, B., Kanter, D., Wu, B., et al. (2021). Fertilizer overuse in Chinese smallholders due to lack of fixed inputs. *Journal of Environmental Management*, *293*, 112913. https://doi.org/10.1016/j.jenvman.2021.112913

Shen, H., Chen, Y., Hu, Y., Ran, L., Lam, S. K., Pavur, G. K., et al. (2020). Intense warming will significantly increase cropland ammonia volatilization threatening food security and ecosystem health. *One Earth*, *3*(1), 126–134. https://doi.org/10.1016/j.oneear.2020.06.015

Shi, M., Fisher, J. B., Brzostek, E. R., & Phillips, R. P. (2016). Carbon cost of plant nitrogen acquisition: Global carbon cycle impact from an improved plant nitrogen cycle in the Community Land Model. *Global Change Biology*, *22*(3), 1299–1314. https://doi.org/10.1111/gcb.13131

Siman, F. C., Andrade, F. V., & Passos, R. R. (2020). Nitrogen fertilizers and NH3 volatilization: Effect of temperature and soil moisture. *Communications in Soil Science and Plant Analysis*, *51*(10), 1283–1292. https://doi.org/10.1080/00103624.2020.1763384

Skamarock, W. C., Klemp, J. B., Dudhia, J., Gill, D. O., Liu, Z., Berner, J., et al. (2019). *A description of the advanced research WRF model version 4.1* (NCAR/TN-556+STR). https://doi.org/10.5065/1dfh-6p97

Slinn, W. G. N. (Ed.) (1984). *Precipitation scavenging*. U.S. Department of Energy.

Song, Y., Tan, M., Zhang, Y., Li, X., Liu, P., & Mu, Y. (2024). Effect of fertilizer deep placement and nitrification inhibitor on N2O, NO, HONO, and NH3 emissions from a maize field in the North China Plain. *Atmospheric Environment*, *334*, 120684. https://doi.org/10.1016/j.atmosenv.2024.120684

Van Damme, M., Clarisse, L., Heald, C. L., Hurtmans, D., Ngadi, Y., Clerbaux, C., et al. (2014). Global distributions, time series and error characterization of atmospheric ammonia (NH 3) from IASI satellite observations. *Atmospheric Chemistry and Physics*, *14*(6), 2905–2922. https://doi.org/10.5194/acp-14-2905-2014

Van Damme, M., Whitburn, S., Clarisse, L., Clerbaux, C., Hurtmans, D., & Coheur, P.-F. (2017). Version 2 of the IASI NH 3 neural network retrieval algorithm: Near-real-time and reanalysed datasets. *Atmospheric Measurement Techniques*, *10*(12), 4905–4914. https://doi.org/10.5194/amt-10-4905-2017

Vira, J., Hess, P., Ossohou, M., & Galy-Lacaux, C. (2022). Evaluation of interactive and prescribed agricultural ammonia emissions for simulating atmospheric composition in CAM-chem. *Atmospheric Chemistry and Physics*, *22*(3), 1883–1904. https://doi.org/10.5194/acp-22-1883-2022

Werner, M., Kryza, M., Geels, C., Ellermann, T., & Skjøth, C. A. (2017). Ammonia concentrations over Europe–application of the WRF-Chem model supported with dynamic emission. *Polish Journal of Environmental Studies*, *26*(3), 1323–1341. https://doi.org/10.15244/pjoes/67340

Wesely, M. (2007). Parameterization of surface resistances to gaseous dry deposition in regional-scale numerical models. *Atmospheric Environment*, *41*, 52–63. https://doi.org/10.1016/j.atmosenv.2007.10.058

Wulahati, A., Cui, X., Cai, H., You, L., & Zhou, F. (2023). Global crop-specific nitrogen fertilization dataset in 1961-2020. https://doi.org/10.11888/Terre.tpdc.300446

Xu, P., Li, G., Zheng, Y., Fung, J. C., Chen, A., Zeng, Z., et al. (2024). Fertilizer management for global ammonia emission reduction. *Nature*, *626*(8000), 792–798. https://doi.org/10.1038/s41586-024-07020-z

Xu, W., Zhao, Y., Wen, Z., Chang, Y., Pan, Y., Sun, Y., et al. (2022). Increasing importance of ammonia emission abatement in PM2. 5 pollution control. *Science Bulletin*, *67*(17), 1745–1749. https://doi.org/10.1016/j.scib.2022.07.021

Yu, G., Jia, Y., He, N., Zhu, J., Chen, Z., Wang, Q., et al. (2019). Stabilization of atmospheric nitrogen deposition in China over the past decade. *Nature Geoscience*, *12*(6), 424–429. https://doi.org/10.1038/s41561-019-0352-4

Zaehle, S., & Friend, A. (2010). Carbon and nitrogen cycle dynamics in the O-CN land surface model: 1. Model description, site-scale evaluation, and sensitivity to parameter estimates. *Global Biogeochemical Cycles*, *24*(1), GB1005. https://doi.org/10.1029/2009GB003521

Zhan, X., Adalibieke, W., Cui, X., Winiwarter, W., Reis, S., Zhang, L., et al. (2020). Improved estimates of ammonia emissions from global croplands. *Environmental Science & Technology*, *55*(2), 1329–1338. https://doi.org/10.1021/acs.est.0c05149

Zhang, L., Chen, Y., Zhao, Y., Henze, D. K., Zhu, L., Song, Y., et al. (2018). Agricultural ammonia emissions in China: Reconciling bottom-up and top-down estimates. *Atmospheric Chemistry and Physics*, *18*(1), 339–355. https://doi.org/10.5194/acp-18-339-2018

Zhang, Y., Mu, Y., Zhou, Y., Tian, D., Liu, J., & Zhang, C. (2016). NO and N2O emissions from agricultural fields in the North China Plain: Origination and mitigation. *Science of the Total Environment*, *551*, 197–204. https://doi.org/10.1016/j.scitotenv.2016.01.209

Zheng, B., Tong, D., Li, M., Liu, F., Hong, C., Geng, G., et al. (2018). Trends in China's anthropogenic emissions since 2010 as the consequence of clean air actions. *Atmospheric Chemistry and Physics*, *18*(19), 14095–14111. https://doi.org/10.5194/acp-18-14095-2018

Zheng, J. Y., Yin, S. S., Kang, D. W., Che, W. W., & Zhong, L. J. (2012). Development and uncertainty analysis of a high-resolution NH_3 emissions inventory and its implications with precipitation over the Pearl River Delta region, China. *Atmospheric Chemistry and Physics*, *12*(15), 7041–7058. https://doi.org/10.5194/acp-12-7041-2012

Zhu, L., Henze, D., Bash, J., Jeong, G.-R., Cady-Pereira, K., Shephard, M., et al. (2015). Global evaluation of ammonia bidirectional exchange and livestock diurnal variation schemes. *Atmospheric Chemistry and Physics*, *15*(22), 12823–12843. https://doi.org/10.5194/acp-15-12823-2015

References From the Supporting Information

Chen, W. H., Jia, S. G., Wang, X. M., Shao, M., Liao, W. H., Guenther, A., et al. (2023). Precipitation trend increases the contribution of dry reduced nitrogen deposition. *npj Climate and Atmospheric Science*, *6*(1), 62. https://doi.org/10.1038/s41612-023-00390-7

Gao, Q., Zhang, X. Y., Liu, L., Lu, X. H., & Wang, Y. Y. (2023). A database of atmospheric inorganic nitrogen deposition fluxes in China from satellite monitoring. *Scientific Data*, *10*(1), 698. https://doi.org/10.1038/s41597-023-02607-z

Huang, B. Y., Thorne, P. W., Banzon, V. F., Boyer, T., Chepurin, G., Lawrimore, J. H., et al. (2017). Extended reconstructed Sea surface temperature, version 5 (ERSSTv5): Upgrades, validations, and intercomparisons. *Journal of Climate*, *30*(20), 8179–8205. https://doi.org/10.1175/JCLI-D-16-0836.1

Erratum

The originally published version of this article omitted the contributions of coauthor Xitian Cai in the author contribution list. They are as follows: Conceptualization; Formal analysis; Investigation; Resources; Supervision; Validation; Writing – review & editing. This may be considered the authoritative version of record.